PNAS RESEARCH ARTICLE | CHEMISTRY

Differences in enantiomeric diffusion can lead to selective chiral amplification

Jean Gillet[a,1], Yves Geerts[b,c], Laurence Rongy[a,1], and Yannick De Decker[a,1]

Edited by Lia Addadi, Weizmann Institute of Science, Rehovot, Israel; received November 10, 2023; accepted March 20, 2024

A fundamental question associated with chirality is how mixtures containing equal amounts of interconverting enantiomers can spontaneously convert to systems enriched in only one of them. Enantiomers typically have similar chemical properties, but can exhibit distinct reactivity under specific conditions, and these differences can be used to bias the system's composition in favor of one enantiomer. Transport properties are also expected to differ for enantiomers in chiral solvents, but the role of such differences in chiral symmetry breaking has not been clarified yet. In this work, we develop a theoretical framework to show that asymmetry in diffusion properties can trigger a spontaneous and selective symmetry breaking in mixtures of enantiomers. We derive a generic evolution equation for the enantiomeric excess in a chiral solvent. This equation shows that the relative stability of homochiral domains is dictated by the difference of diffusion coefficients of the two enantiomers. Consequently, deracemization toward a specific enantiomeric excess can be achieved when this difference is large enough. These results hold significant implications for our understanding of chiral symmetry breaking.

homochirality | deracemization | nonlinear chemistry | reaction–diffusion | origin of life

Significance

One of the central problems associated with the origin of life is how chiral symmetry was broken. Several mechanisms, such as directed or spontaneous chiral symmetry breaking, have been proposed to explain why specific classes of enantiomers have been overwhelmingly favored under prebiotic conditions. In this study, we demonstrate that having enantiomers with different diffusion coefficients can be sufficient to bias the final enantiomeric composition of reactive systems, up to complete deracemization. This result is significant because it provides a mechanism for chiral selection and amplification that relies on diffusion asymmetries.

Chirality, the property that objects cannot be superimposed onto their mirror image, plays a pervasive role across various scientific fields. Chirality can be considered as important as mass or energy, because it is a fundamental property that shapes the universe and the living world.

At the molecular level, chirality has profound consequences on intermolecular interactions (1) and, thus, on the functioning of living systems. Life as we know it relies on large organic compounds, and chiral molecules swiftly outnumber achiral ones when molecules possess more than eight carbon atoms (2). As a result, life depends on chiral building blocks and chirality naturally affects the structure, function, and recognition of large biological molecules (3). The importance of chirality becomes evident in the context of drug design and development, as exemplified by the unfortunate case of thalidomide in the 1950s and 1960s, where one of its enantiomers caused fetal abnormalities (4). Chirality should not be seen as a static property, but rather as a dynamic one. Many molecules can switch between different chiral conformations, referred to as enantiomers (5). This dynamic interconversion leads some molecular systems to undergo racemization, a process converting a system containing one enantiomer into a mixture of an equal amount of both forms. The reverse process, known as deracemization, can also occur, but it requires nonequilibrium constraints (6). Deracemization can be considered a form of chiral symmetry breaking (CSB) since the system transforms from a globally achiral state to a chiral one.

A central question surrounding deracemization is how to bias CSB toward a desired enantiomer. Nature has selected a specific handedness for the building blocks of life (7), but the mechanisms behind such selectivity are still unclear. In man-made experiments, external biases like circularly polarized light (8), slight initial enantiomeric excesses, the addition of another chiral molecule (9), and contact with a chiral surface (10) can be used to direct CSB. When exposed to such bias, a racemic system, far enough from thermodynamic equilibrium, self-enriches into an excess of one specific enantiomer through a process known as chiral amplification (1). Chiral amplification is thought to occur, for example, in the autocatalytic Soai reaction (11) and during Viedma ripening (12). Many instances of chemical systems undergoing directed deracemization have, since then, been discovered (13).

Regardless of the bias used and the chiral amplification mechanism involved, it is commonly believed that directed CSB occurs because the reaction (or crystallization) rate becomes larger for one enantiomer than for the other, making CSB a reaction-driven phenomenon. To the best of our knowledge, directed deracemization has

Author affiliations: [a]Nonlinear Physical Chemistry Unit, Faculté des Sciences, CP – 231, Université libre de Bruxelles, Bruxelles 1050, Belgium; [b]Laboratoire de Chimie des Polymères, Faculté des Sciences, Université libre de Bruxelles, Bruxelles 1050, Belgium; and [c]International Solvay Institutes of Physics and Chemistry, Université libre de Bruxelles, Bruxelles 1050, Belgium

Author contributions: J.G., Y.G., L.R., and Y.D.D. designed research; J.G. performed research; J.G. contributed new reagents/analytic tools; J.G., L.R., and Y.D.D. analyzed data; Y.G. contributed to the interpretation of the results and the improvement of the article; and J.G., Y.G., L.R., and Y.D.D wrote the paper.

The authors declare no competing interest.

This article is a PNAS Direct Submission.

[1]To whom correspondence may be addressed. Email: Jean.Gillet@ulb.be, Laurence.Rongy@ulb.be, or Yannick.De.Decker@ulb.be.

This article contains supporting information online at https://www.pnas.org/lookup/suppl/doi:10.1073/pnas.2319770121/-/DCSupplemental.

Published April 18, 2024.

never been considered to result from differences in the diffusion rates of enantiomers. Enantioselective diffusion and elution processes demonstrate such differences, leading to the separation of enantiomers using various techniques such as permeation through chiral membranes or chiral chromatography (14–17). These systems create a chiral environment in which the enantiomers experience different diasteroisomeric interactions and forces that affect their mobility (14). Experimental measurements have quantified this difference in mobility. For example, Aoki et al. reported the enantioselective permeation of various racemates through a chiral polymeric membrane (18). The ratio of diffusion coefficients of enantiomers ranged from 1.2 to 3.6, indicating a high degree of enantioselectivity. Hovorka et al. measured the permeability and diffusion coefficients of methyl lactate enantiomers in cellophane membranes (19). They found that the ratio of diffusion coefficients of L-methyl lactate and D-methyl lactate could be as large as 9.4. Theoretical works and model calculations (20, 21), and subsequent experiments in chiral nematic liquid crystals highlighted enantiomer differentiation by migration (22, 23). For instance, Jiang and Yang showed that the diffusion coefficient of a chiral species is doubled when moving from a medium of opposite chirality to a medium of the same chirality (22).

In this work, we demonstrate that such differences in the diffusion coefficients can lead to directed deracemization. First, we introduce a generic reaction–diffusion equation for the evolution of the enantiomeric composition in a chiral medium. This equation allows to identify the parameters influencing the relative stability of two domains with different composition. We conclude from this analysis that asymmetries in diffusion rates play a role in the competition between domains of opposite chirality that is as significant as the one played by asymmetric chemical reactivities. Second, we show that diffusion-driven deracemization can be achieved for several classes of models of CSB, provided that the difference in diffusion coefficients is large enough. These results open up perspectives for controlling and elucidating deracemization processes, as discussed at the end of this article.

Theoretical Framework

Deracemization is a dissipative phenomenon studied in the framework of nonequilibrium thermodynamics. Far away from equilibrium, racemic mixtures can become unstable and be replaced by scalemic states, i.e., mixtures with an unbalanced ratio of enantiomer concentrations. These states can be sustained through a constant supply of energy and matter from the environment. Theoretical models were proposed to gain insight into the mechanisms behind deracemization (1, 24). These models typically explore the competition between two enantiomers, which we will denote as R and S. They include reactive events that result in a modification of the number of particles of the species involved, and to an interconversion between enantiomers. In some cases, transport processes, often in the form of diffusion, are also considered. Both deterministic reaction–diffusion equations and stochastic approaches have been used in these models.

The observed mechanism underlying CSB can be summarized as follows: An initial random fluctuation of composition undergoes amplification through autocatalytic kinetics, where one of the enantiomers enhances its own rate of production. Diffusion was found to influence the transients leading to the final scalemic states, because it controls the rate at which domains enriched in one enantiomer propagate over space (25–27). If the reaction kinetics and rate constants are the same for both enantiomers, and if the initial fluctuations of composition are random, these systems will tend to have equal probabilities of reaching states enriched in either R or S. Biases have to be introduced in those models to induce directed deracemization, often by including asymmetries in the reaction kinetics (28). Here, we show on the basis of a generic class of reaction–diffusion models of CSB that this symmetry can also be broken if two enantiomers have different diffusion coefficients. Consequently, directed deracemization can be achieved even in the absence of kinetic bias.

We consider isothermal systems containing two enantiomers, R and S, in a chiral solvent. The evolution equations for their local concentrations, r and s, are assumed to be of the reaction–diffusion type:

$$\frac{\partial r}{\partial t} = f(r,s) + D_R \nabla^2 r, \qquad [1]$$

$$\frac{\partial s}{\partial t} = g(r,s) + D_S \nabla^2 s. \qquad [2]$$

Here, $f(r,s)$ and $g(r,s)$ are kinetic terms that contain contributions associated with chemical reactions, interconversion, exchanges with the environment, etc. The second terms represent Fickian diffusion with constant diffusion coefficients. Because we consider chiral solvents, we expect the diffusion coefficients of species R and S, respectively D_R and D_S to differ. To highlight such difference, we introduce an adimensional parameter $\gamma = (D_R - D_S)/(D_R + D_S)$ and rewrite the diffusion coefficients as $D_R = D(1+\gamma)$ and $D_S = D(1-\gamma)$, respectively, where $D = (D_R + D_S)/2$ is the average diffusion coefficient. The diffusive asymmetry parameter γ ranges from -1 to 1, and is 0 for enantiomers having identical diffusion coefficients. As an illustration, the ratios of diffusion coefficients reported by Aoki et al. would result in $\gamma = \pm(0.09 - 0.56)$ (18) and those of Hovorka et al. would give $\gamma = \pm 0.81$ (19).

Next, we define the enantiomeric excess $u = r - s$, and the total concentration, $v = r + s$. Using Eqs. **1** and **2**, the evolution equations for these quantities read

$$\frac{\partial u}{\partial t} = f(u,v) - g(u,v) + D\nabla^2 u + D\gamma \nabla^2 v, \qquad [3]$$

$$\frac{\partial v}{\partial t} = f(u,v) + g(u,v) + D\nabla^2 v + D\gamma \nabla^2 u. \qquad [4]$$

In many cases, a quasi-steady-state approximation can be assumed for the local kinetic term of the total concentration v (28), meaning that $f(u,v) + g(u,v) \approx 0$. This condition implies that v evolves over time scales that are shorter than those of u. This assumption often holds because f and g contain autocatalytic terms that are very much alike, since enantiomers have similar reactivity. This means that the total concentration evolves rapidly compared to the difference of concentrations as long as one starts from an almost racemic composition, where $u \approx 0$. Assuming $f(u,v) + g(u,v) = 0$ leads to an expression for $v = \tilde{v}(u)$ which can be injected in Eq. **3**. Defining $\Phi(u) = f(u,\tilde{v}(u)) - g(u,\tilde{v}(u))$, the evolution equation for u now reads

$$\frac{\partial u}{\partial t} = \Phi(u) - \nabla \cdot \bar{J}, \qquad [5]$$

in which

$$\bar{J} = -D\,(1 + \gamma\,\tilde{v}_u)\,\nabla u \qquad [6]$$

is a diffusion flux, and where the subscript denotes differentiation with respect to u. We note that the evolution law for the enantiomeric excess u is also of the reaction–diffusion type, but where diffusion is effectively nonideal. $D\,(1+\gamma\,\tilde{v}_u)$ plays the role of a variable diffusion coefficient whose value depends on the degree of diffusive asymmetry γ, but also on the local value of the enantiomeric excess through $\tilde{v}_u$.

Eq. **5** is very general, but there is a particular instance of this equation that deserves attention. Most models for CSB, such as Frank-like models (29), the Kondepudi model (28) and the cyclic limited enantioselectivity model (30), utilize symmetric kinetic equations in which $f(r,s) = g(s,r)$. Because of this symmetry with respect to permutation, all these models present a pitchfork bifurcation in the vicinity of which the dimensionless evolution law for u becomes

$$\frac{\partial u}{\partial t} = \lambda\, u - u^3 + \nabla\cdot\left[(1+2\,\gamma\,u)\,\nabla u\right], \qquad [7]$$

where λ is a combination of constants specific to the models (see *SI Appendix*, section 1 for more details). Eq. **7** can be seen as the normal form of the evolution equation for u in the case of symmetric kinetics. It should be noted that the kinetic laws of models for CSB during crystallization, Soai's reaction or polymerization processes can also be reduced to an equation of this type [*SI Appendix*, section 1 and (24, 31–33)]. It admits three homogeneous stationary states, $u = 0$, and $u = \pm\sqrt{\lambda}$, which merge at the critical point $\lambda_c = 0$. The parameter λ thus controls the system's distance from criticality. While λ is often a complex combination of model-specific parameters, it can be shown to increase with the concentration of a precursor for both enantiomers, in the Kondepudi and in the cyclic LES models (*SI Appendix*, section 1). In this context, it can be interpreted as a parameter that quantifies how the rate of synthesis of R and S compares with that of other processes.

Competition between Domains of Opposite Handedness

To investigate the influence of diffusive asymmetry on CSB, we will explore the evolution of an interface separating a stable S-rich domain with enantiomeric excess u_- and a stable R-rich domain with enantiomeric excess u_+. In the case of symmetric kinetics, this situation corresponds to a system operating beyond the bifurcation point, with two spatial regions having opposite enantiomeric excess values (for systems obeying Eq. **7**, $-\sqrt{\lambda}$ and $+\sqrt{\lambda}$, respectively). In the more general case, the values of u in the two domains would have opposite signs, but could have different absolute values.

The direction of propagation of this interface will reveal the relative stability of these domains and, thus, the selectivity of the system toward one of the enantiomers. Starting from Eq. **5**, we find (*Materials and Methods*) that for spatially isotropic systems the velocity c of such an interface is given by

$$c = \frac{\Delta\mathcal{F}}{\sigma} - D\,\gamma\,\frac{A}{\sigma} - \overline{D}\,\frac{(d-1)}{\eta}. \qquad [8]$$

In this general equation, A and σ are constants depending on the shape of the interface, $d = 1, 2$ or 3 represents the spatial dimension of the system, and η is the radius of curvature of the S-rich domain. The quantity $\overline{D}$ denotes the spatial average of the effective diffusion coefficient $D\,(1+\gamma\,\tilde{v}_u)$. $\mathcal{F} = -\int \Phi(u)\,du$ corresponds to the kinetic potential of the local evolution law, whose minima correspond to stable steady states of the system, and $\Delta\mathcal{F} = \mathcal{F}(u_+) - \mathcal{F}(u_-)$ is the difference of kinetic potential between the two nonracemic states. This quantity is zero in the case of symmetric kinetic laws, is positive when u_- is more stable than u_+, and is negative otherwise. Note that when $\gamma = 0$, $\overline{D}$ becomes the diffusion coefficient of the two species involved and one recovers the classical prediction for the front velocity between two stable states (34).

The first term in Eq. **8** indicates that asymmetric evolution laws, which induce an asymmetry in the values of the homogeneous steady states, lead to the propagation of the interface in favor of one of the enantiomers. The two other contributions are related to diffusion. The third term shows that curved (concave) domains tend to shrink. The second term is the most important for our purpose: It shows that the sign of c and, thus the direction of propagation of the interface, is also controlled by the magnitude and sign of γ, which measures the asymmetry of diffusion between species R and S.

Without Kinetic Asymmetries. To illustrate this effect, we first consider the case of symmetric kinetics ($\Delta\mathcal{F} = 0$) without curvature-related effects (a planar interface or, equivalently, a 1-dimensional system). We also consider system obeying dimensionless Eq. **7**. In this case, the dimensionless propagation velocity becomes $c = -\gamma\,A/\sigma$. For moderate values of γ, we can expect the profile $u(z)$ to be close to the solution for $\gamma = 0$, denoted $u^0(z)$, which represents the profile of an immobile interface (Fig. 1). This assumption allows us to evaluate A and σ explicitly (*SI Appendix*, section 4).

We performed numerical integrations of the dimensionless evolution law for u, Eq. **7**, as well as the aforementioned models for symmetric kinetics (a Frank-like model, the Kondepudi model, and the cyclic limited enantioselectivity model). In the vicinity of their pitchfork bifurcations, these models obey Eq. **7**, whose stationary interface is given by $u^0(z) = (u_- + u_+\,e^{\kappa z})/(1+e^{\kappa z})$, with $\kappa = (u_+ - u_-)/\sqrt{2}$ (see ref. 35 and *Materials and Methods*). The first derivative u^0_z is always positive and the profile has an inflection point at $z = 0$, as shown in Fig. 1. With this information, we can evaluate the dimensionless front velocity, which is given by $c = -2\sqrt{2}\,\gamma\,\lambda/5$ (see *SI Appendix*, section 4 for more details). Consequently, the enantiomer that diffuses the fastest will invade the entire system.

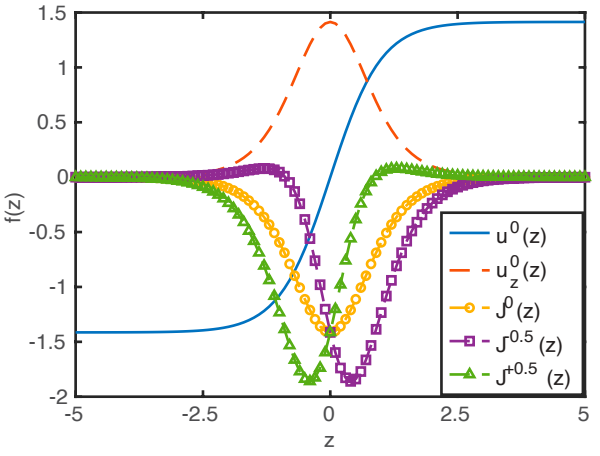

Fig. 1. Plot of the profile solution u^0, u^0_z and diffusion fluxes J as a function of the coordinate z, i.e., the direction separating the enantiomers. Three different values of γ are shown for J: $\gamma \pm 0.5$ and $\gamma = 0$. $\lambda = 2$.

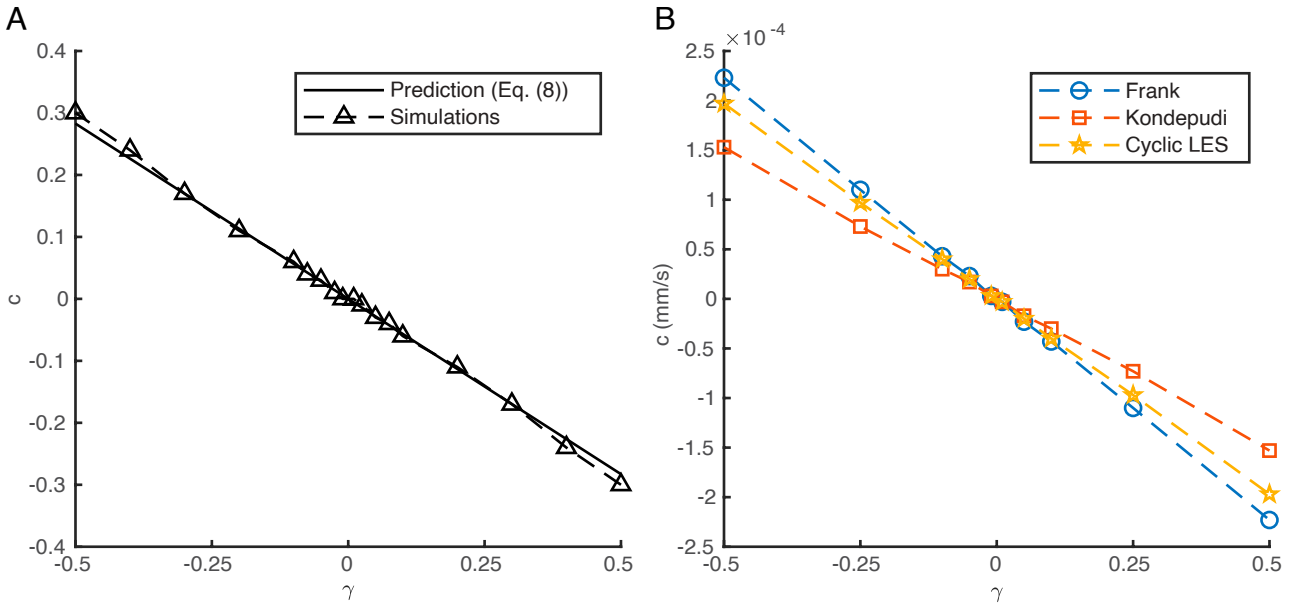

Fig. 2. Front propagation velocity as a function of the diffusive asymmetry parameter in 1-dimensional systems with symmetric kinetics ($\Delta\mathcal{F} = 0$). (*A*) Comparison of the dimensionless front propagation velocity c as a function of the diffusive asymmetry parameter γ obtained from numerical integrations of dimensionless Eq. **7** with predictions from Eq. **8**. Considering the stationary interface $u^0(z)$, Eq. **8** predicts a dimensionless propagation velocity c that evolves according to $c = -2\sqrt{2}\gamma\lambda/5$ (solid black line). A good agreement is observed between simulations and predictions. Simulations parameters: $\lambda = 1.0$, total simulation time $= 10$ and system size was $L = 100$, with temporal (dt) and spatial (dx, dy) step sizes set to 1.0×10^{-5} and 0.01, respectively. (*B*) Dimensional front propagation velocity c as a function of the diffusive asymmetry parameter γ for three classes of models. Results from numerical simulations of Frank-like (29), Kondepudi (28) and cyclic limited enantioselectivity model (LES) models (30). All three different models exhibit a linear relationship. More detail on the equations integrated, kinetic rates values, and simulation parameters are available in *SI Appendix*, section 2. Associated time scales are provided in *SI Appendix*, section 5. Dashed lines are guides for the eye.

If $D_R < D_S$, $\gamma < 0$ and c is positive: The S-rich state u_-, initially located at $z < 0$, invades the R-rich state u_+, initially located at $z > 0$ (and vice versa for positive values of γ). This predicted linear relationship between c and γ is in excellent agreement with numerical integrations of Eq. **7**, as shown in Fig. 2*A*. Interestingly, a linear relationship is also observed for the three models considered here (Fig. 2*B*), even for large diffusive asymmetries.

With Kinetic Asymmetries. When kinetic asymmetries are present, $\Delta\mathcal{F} \neq 0$ and the fate of the interface will be decided by a balance between kinetics and diffusive asymmetries. Consider as an illustration the case where the S-rich state is the most stable in well-mixed systems, which translates into $\Delta\mathcal{F} > 0$. For 1-dimensional systems and in the absence of diffusive asymmetry, $c > 0$ and the S-rich domain invades the other one. This relative stability can be reversed for sufficiently positive values of γ, that is when R diffuses faster than S, because c becomes negative whenever $\gamma > \Delta\mathcal{F}/A$. This means that R can dominate if it diffuses faster than S, even when S is the kinetically favored enantiomer.

Higher-Dimensional Systems. The situation becomes more complex for nonplanar interfaces. In the presence of curvature effects, the dominating enantiomer is not necessarily the one that diffuses faster, even when the two enantiomers have identical evolution laws ($\Delta\mathcal{F} = 0$). Consider for example the three models mentioned above, but in a 2-dimensional system where a circular S-rich domain of radius η is surrounded by an R-rich environment. In this case, Eq. **8** reduces to $c = -D\gamma A/\sigma - \overline{D}/\eta$. This equation predicts the existence of a critical radius, corresponding to $c = 0$. For systems obeying Eq. **7**, this critical radius is given by

$$\eta_c = -\frac{5}{2\sqrt{2}\gamma\lambda}, \qquad [9]$$

(*SI Appendix*, section 4). Only S-rich nuclei with a radius larger than η_c will grow over time; smaller nuclei will disappear, even though S diffuses faster than R. The critical radius depends on the distance from the bifurcation point through λ, and on the asymmetry of diffusion rates through γ. Notably, since γ can be negative, if λ becomes increasingly large, the critical radius will tend toward 0. This implies that when S diffuses faster than R, a domain in the S-rich state will invade the system, regardless of its size, effectively removing the existence of a critical nucleus.

Directed Chiral Symmetry Breaking

We will now demonstrate that directed CSB can be achieved when starting from a globally achiral system. As a first illustration, the time evolution of a 2-dimensional system obeying Eq. **7**, is shown in Fig. 3. The two lines depict simulations performed with an identical initial condition, which corresponds to small random fluctuations around a racemic composition ($u = 0$). The first line shows the evolution of a system where the diffusion coefficients of the two enantiomers are identical, so that $\gamma = 0$. We observe that the R-rich u_+ state dominates for long times. For this case, an average over 1,000 simulations with random initial conditions gives ≈50% of R-states. As can be seen in the second line, the final state of the system can be directed toward the S-rich u_- state when S diffuses faster than R ($\gamma < 0$). This change aligns with our previous finding that the relative stability of domains of opposite chirality is influenced by asymmetries of diffusion.

The example provided in Fig. 3 corresponds to a specific initial condition. A more general view on the effect of diffusive asymmetry requires statistics over the probability to reach either

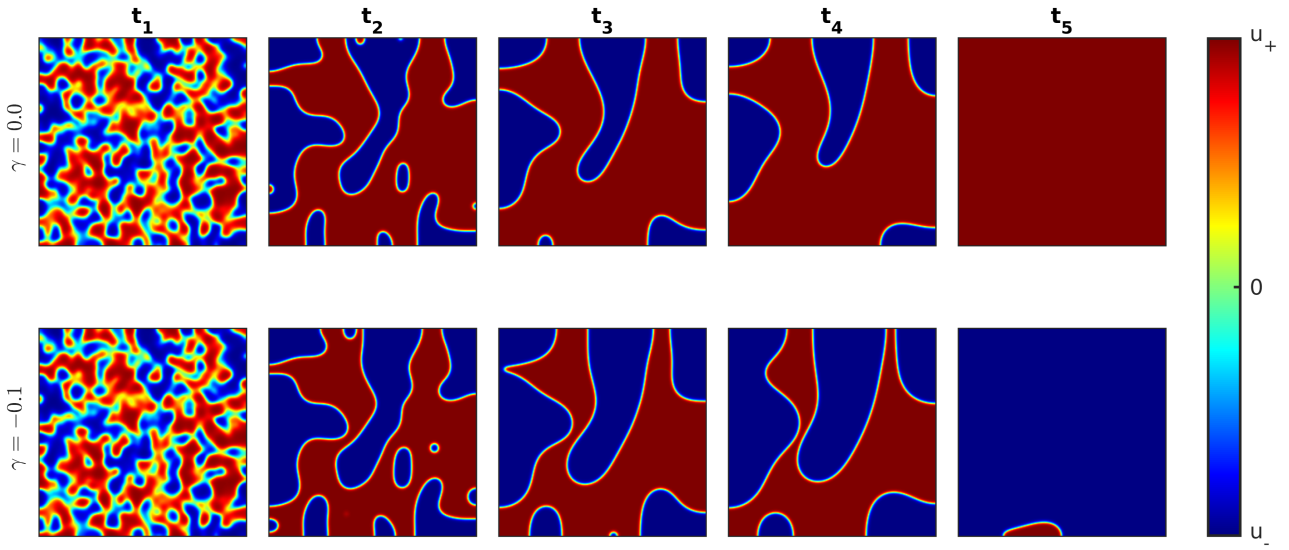

Fig. 3. Evolution of u over time in a 2-dimensional system, obtained from numerical simulations of Eq. **7**. The initial system is a racemic mixture where local perturbations are introduced. Homochiral domains are formed rapidly and then compete to reach a single homogeneous homochiral composition. Parameter values: $\lambda = 0.5$, $\gamma = 0$ (*Upper* line) and $\gamma = -0.1$ (*Bottom* line), size of the system $L_x = L_y = L = 250$, and total simulation time = 15,000 with temporal (dt) and spatial (dx, dy) step sizes set to 0.1 and 1.0, respectively. The concentration scales range from $u_- = -0.7071$ to $u_+ = 0.7071$. Snapshots have been taken at various times: $t_1 = 30$, $t_2 = 150$, $t_3 = 375$, $t_4 = 600$, and $t_5 = 3{,}000$.

an S-rich or an R-rich state. Fig. 4 plots the probability to reach the R-rich state as a function of γ (Fig. 4*A*) and λ (Fig. 4*B*), for 2-dimensional systems obeying the normal form Eq. **7**. Since all simulations start from random fluctuations around the racemic state, this probability will be of 50% when $\gamma = 0$, because states u_+ and u_- have identical stability*. However, we have seen that the stability of R-rich regions is enhanced if $\gamma > 0$. In particular, we showed the existence of a critical distance from the bifurcation point where R-rich or S-rich clusters will grow, whatever their size. This situation is reflected in the statistics of Fig. 4. We observe that the fraction of systems ending in the R-rich state rapidly increases when operating sufficiently far from the

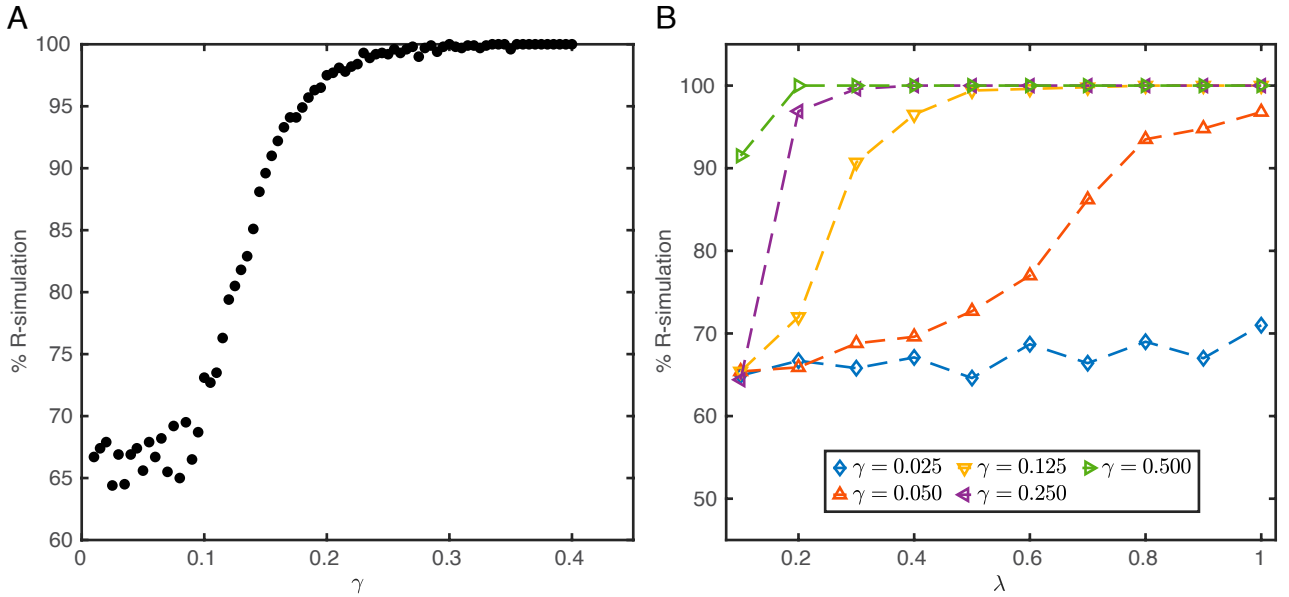

Fig. 4. (*A*) Probability to obtain R-homochiral states from racemic mixtures as a function of γ, for a given value of $\lambda = 0.5$. Results obtained with negative values of γ are symmetrical. (*B*) Probability to obtain R-homochiral states from racemic mixtures as a function of λ, for different values of the diffusive asymmetry parameter γ. Results are obtained from numerical integrations of Eq. **7** in 2-dimensional systems with the same sizes and integration parameters as in Fig. 3. Each point is obtained from 1,000 simulations starting from racemic initial conditions randomly distributed in space. Full selectivity can be achieved starting from $\gamma = 0.25$ and $\lambda \geq 0.5$. When $\gamma = 0$, there is an equal probability to obtain R- or S-homochiral states (% R-simulations $\approx$ 50%). When the same type of simulations are conducted for Frank-like, Kondepudi, and cyclic LES models in 1-dimensional systems, the same trends are observed (*SI Appendix*, section 3). Dashed lines are guides for the eye.

*It should be noted that as $\gamma \to 0$, some realizations of these simulations do not lead to global homochirality, but rather to a coexistence of homochiral domains, as was also observed in ref. 25.

bifurcation point or with sufficiently large diffusive asymmetries. The combination of diffusive asymmetry and nonequilibrium constraints results in an almost perfect control of the chirality in the system.

Discussion

Chiral symmetry breaking holds crucial importance in chemistry and beyond. In synthetic chemistry, a precise control of the chiral outcome in enantiomeric mixtures is often necessary. The mechanisms underlying this symmetry breaking have probably also played an important role in the emergence of biohomochirality. This work demonstrates that an asymmetry in diffusion rates can induce directed CSB, favoring one enantiomer. Such asymmetry can be caused by the presence of a chiral solvent in the system. Interestingly, the required degree of diffusive asymmetry is not extreme: Numerical simulations suggest that an absolute value of γ around 0.2 is sufficient to achieve nearly 100% conversion to a chosen enantiomeric excess state. As a reminder, experimental values from the literature indicate that this parameter can range between 0.09 and 0.81 (18, 19). Simulations of the Kondepudi model also show that diffusive asymmetry leads to deracemization of a centimeter-sized system within a few minutes, when parameter values consistent with Soai's reaction are used (*SI Appendix*, section 5). Therefore, we believe that diffusion-controlled directed CSB is within experimental reach.

Additionally, our results may shed light on existing experimental examples of CSB, such as the Soai reaction (9) or Viedma deracemization (12). It may also offer insight into the chiral self-sorting experiments reported by Dressel et al. (36) where a racemic mixture of helical enantiomers can spontaneous separate into two chiral domains with opposite handedness. These processes heavily rely on diffusion, as they involve the formation and dissolution of crystals or molecular aggregates that can selectively incorporate or exclude one enantiomer. Minor differences in enantiomer diffusion coefficients may thus play an important role in the amplification mechanisms driving these systems.

More generally, diffusive asymmetries are expected to play a significant role in chiral recognition and separation in complex media. For instance, chiral chromatography, which uses a chiral stationary phase that preferentially interacts with one of the enantiomers, and chiral membrane separation strongly rely on the modification of enantiomer transport properties, including diffusivity (14–17). Our framework offers a path to a global understanding of the role played by diffusive asymmetries in these separation processes. More specific models could be developed to describe all these experiments in detail (37, 38).

In conclusion, our main message is that differences in diffusion coefficients between enantiomers can be exploited to control the chirality of a system. While theoretical models and numerical simulations support this claim, we hope that this work triggers corresponding experiments. We suggest focusing experimental efforts to verify our prediction on systems with interconverting enantiomers, in chiral media where diffusion is the main transport phenomenon, such as chiral gels.

Materials and Methods

General Expression for the Front Velocity. In this section, we derive Eq. **8** of the main text. We start by considering a 1-dimensional system, in which the enantiomeric excess obeys the general evolution law Eq. **5** of the main text:

$$\frac{\partial u}{\partial t} = \Phi(u) + \frac{\partial}{\partial x}\left[D\,(1+\gamma\,\tilde{v}_u)\,\frac{\partial u}{\partial x}\right]. \quad [10]$$

We introduce a frame moving at a constant velocity c, whose coordinate is given by $z = x - c\,t$. The evolution law for u becomes

$$-c\,u_z = \Phi(u) + [D\,(1+\gamma\,\tilde{v}_u)\,u_z]_z\,, \quad [11]$$

where, for simplicity, we use subscripts to denote differentiation. We now multiply both sides of Eq. **11** by u_z and integrate over z. This yields:

$$c\int_{-\infty}^{+\infty}(u_z)^2\,dz = \Delta\mathcal{F} - \int_{-\infty}^{+\infty}[D\,(1+\gamma\,\tilde{v}_u)\,u_z]_z\;u_z\,dz, \quad [12]$$

in which

$$\begin{aligned}\Delta\mathcal{F} &= -\int_{-\infty}^{+\infty}\Phi(u)\,u_z\,dz\\ &= -\int_{u_-}^{u^+}\Phi(u)\,du\\ &\equiv \mathcal{F}(u_+) - \mathcal{F}(u_-),\end{aligned} \quad [13]$$

The second contribution can be simplified by noting that

$$\int_{-\infty}^{+\infty}[D\,(1+\gamma\,\tilde{v}_u)\,u_z]_z\;u_z\,dz = D\underbrace{\int_{-\infty}^{+\infty}u_{zz}\,u_z\,dz}_{\mathrm{I}} \quad [14]$$

$$+\,D\,\gamma\underbrace{\int_{-\infty}^{+\infty}(\tilde{v}_u\,u_z)_z\,u_z\,dz}_{\mathrm{II}}\,. \quad [15]$$

Since the space derivatives vanish at infinity, the first term I is zero:

$$\mathrm{I} = \left[(u_z)^2\right]_{-\infty}^{+\infty} - \int_{-\infty}^{+\infty}u_{zz}\,u_z\,dz \quad [16]$$

$$= -\mathrm{I} = 0. \quad [17]$$

Expanding II gives

$$\mathrm{II} = \int_{-\infty}^{+\infty}((\tilde{v}_u)_z\,u_z + \tilde{v}_u\,u_{zz})\,u_z\,dz \quad [18]$$

$$= \int_{-\infty}^{+\infty}(\tilde{v}_u)_z\,(u_z)^2\,dz + \int_{-\infty}^{+\infty}\tilde{v}_u\,u_z\,u_{zz}\,dz. \quad [19]$$

Integrating the first term by parts yields

$$\int_{-\infty}^{+\infty}(\tilde{v}_u)_z\,(u_z)^2\,dz = \underbrace{\left[(u_z)^2\,\tilde{v_u}\right]_{-\infty}^{+\infty}}_{=0} - 2\int_{-\infty}^{+\infty}\tilde{v}_u\,u_z\,u_{zz}\,dz. \quad [20]$$

Therefore, we have

$$\begin{aligned}\mathrm{II} &= \int_{-\infty}^{+\infty}(\tilde{v}_u)_z\,(u_z)^2\,dz - \frac{1}{2}\int_{-\infty}^{+\infty}(\tilde{v}_u)_z\,(u_z)^2\,dz,\\ &= \frac{1}{2}\int_{-\infty}^{+\infty}(\tilde{v}_u)_z\,(u_z)^2\,dz \equiv A.\end{aligned} \quad [21]$$

Inserting II in Eq. **12** gives the following expression for the speed of propagation:

$$c = \frac{\Delta\mathcal{F} - D\,\gamma\,A}{\sigma}, \quad [22]$$

where we defined

$$\sigma \equiv \int_{-\infty}^{+\infty}(u_z)^2\,dz \geq 0. \quad [23]$$

In more than 1 dimension, curvature effects must be accounted for. We introduce polar coordinates (η,θ) in 2d, where η is the radius and θ the polar angle. For 3d systems, we can introduce spherical coordinates (η,θ,ϕ), in which ϕ is the azimuthal angle. In any case, in the absence of gradients along θ and ϕ (what we call isotropic systems), the evolution equation becomes

$$\frac{\partial u}{\partial t} = \Phi(u) + D\,\frac{\partial^2}{\partial \eta^2}\,(u+\gamma\,\tilde{v}) + \frac{D\,(d-1)}{\eta}\,\frac{\partial}{\partial \eta}\,(u+\gamma\,\tilde{v}), \qquad [24]$$

where d is the spatial dimension. To obtain an analytical expression for the front velocity, we focus on situations where the radius is large, so that η can be considered constant. We can thus write

$$u_t = \Phi(u) + D\left[(u+\gamma\,\tilde{v})_\eta + \frac{(d-1)}{\eta}\,(u+\gamma\,\tilde{v})\right]_\eta, \qquad [25]$$

where subscripts denote differentiation. The derivative with respect to η appearing in this equation takes the form

$$(u+\gamma\,\tilde{v})_\eta = u_\eta + \gamma\,\tilde{v}_u\,u_\eta = (1+\gamma\,\tilde{v}_u)\,u_\eta. \qquad [26]$$

To summarize, we have an evolution equation of the type

$$u_t = \Phi(u) - J_\eta, \qquad [27]$$

with an effective flux

$$J = -D\,(1+\gamma\,\tilde{v}_u)\,u_\eta - D\,\frac{(d-1)\,(u+\gamma\,\tilde{v})}{\eta}. \qquad [28]$$

We notice that this total flux is the sum of a term which is identical to what we had in 1-dimensional systems, and a correction term that takes curvature into account. Since η is a radius, the boundaries of the spatial domain are 0 and $+\infty$. We consider no-flux boundary conditions and, since we focus on large radius values, the values of u at 0 and at $+\infty$ can be taken to be equal to u_- and u_+, respectively. Introducing a new comoving frame $\zeta = \eta - c\,t$, Eq. **27** reads

$$-c\,u_\zeta = \Phi(u) - J_\zeta. \qquad [29]$$

Multiplying both sides of this equation by u_ζ and integrating over ζ yields:

$$-c\int_{-\infty}^{+\infty}(u_\zeta)^2\,d\zeta = \int_{-\infty}^{+\infty}\Phi(u)\,u_\zeta\,d\zeta - \int_{-\infty}^{+\infty}J_\zeta\,u_\zeta\,d\zeta.$$

Dividing both sides by $-\sigma = -\int_{-\infty}^{+\infty}(u_\zeta)^2\,d\zeta$, the first term in the right-hand side will give the right-hand side of Eq. **22**, and we thus conclude that

$$c = \frac{\Delta\mathcal{F}}{\sigma} - D\,\gamma\,\frac{A}{\sigma} - \overline{D}\,\frac{(d-1)}{\eta}, \qquad [30]$$

where

$$\overline{D} = \frac{\int_{-\infty}^{+\infty} D\,(1+\gamma\,\tilde{v}_u)\,(u_\zeta)^2\,d\zeta}{\int_{-\infty}^{+\infty}(u_\zeta)^2\,d\zeta} \qquad [31]$$

can be seen as a weighted average of the diffusion coefficient $D\,(1+\gamma\,\tilde{v}_u)$. Note that because $D\,(1+\gamma\,\tilde{v}_u)$ plays the role of an effective diffusion coefficient in our framework, we must limit ourselves to cases where this quantity is positive. Consequently, $\overline{D}$ will be positive as well.

Stationary Fronts for Symmetric Kinetics and Diffusion. We look for self-similar solutions $u(z)$ of the 1-dimensional problem, which obey the following boundary conditions:

$$u(z) = \begin{cases} u_- & z \to -\infty \\ u_+ & z \to +\infty. \end{cases} \qquad [32]$$

We consider more specifically the case of symmetric diffusion ($\gamma = 0$). Eq. **11** reduces to

$$-c\,u_z = \Phi(u) + u_{zz}, \qquad [33]$$

where Φ is a cubic polynomial of u with no constant term whenever one considers symmetric kinetic equations and systems close to the critical point (*SI Appendix*, section 1). In such cases, the propagation speed of the fronts is known to be proportional to $u_+ + u_- - 2\,u_0$, which in our case is equal to 0 because of the symmetry of the steady states. We should thus expect domains of opposite handedness to coexist indefinitely in these situations ($c = 0$). Moreover, one can verify by substitution that this stationary front is characterized by a profile of the form

$$u^0(z) = \frac{u_- + u_+\,e^{\kappa\,z}}{1+e^{\kappa\,z}}, \qquad [34]$$

where $\kappa = (u_+ - u_-)/\sqrt{2\,D}$. A similar reasoning also applies for the stationary profile in higher dimensional systems, where ζ replaces z.

Numerical Simulations. Results shown in Figs. 2–4 have been obtained using numerical integrations (39). All equations were numerically integrated using either fourth-order Runge–Kutta or Euler schemes and finite differences were used for spatial discretization. One-dimensional and two-dimensional systems were investigated with no-flux boundary conditions. For the latter, we used a square system such that the length L_x and the width L_y are equal ($L_x = L_y = L$). Evolution equations of a Frank-like (29), the Kondepudi (28) and the cyclic limited enantioselectivity (LES) model (40) have been numerically integrated for Fig. 2*B* in 1-dimensional systems. Coexisting domains of opposite handedness were used as initial conditions. The front velocity was numerically computed from the displacement of the front and plotted against γ. The evolution equations and the parameter values used are provided in *SI Appendix*, section 2. Figs. 3 and 4 have been obtained from numerical integration of Eq. **7** of the main text in 2-dimensional systems. In these systems, the initial conditions in each cell were independently sampled from a Gaussian distribution centered on $u = 0$, and with a standard deviation of 0.01.

Further Material. The symmetry of the evolution equations for r and s implies that the bifurcation of the enantiomeric excess u will also be symmetric, unless there is a kinetic bias. We prove this property in *SI Appendix* for the three aforementioned models. Distributions of probability to obtain R-homochiral states from racemic conditions are also featured for these three models in 1-dimensional systems. Then, we demonstrate the dimensionless expressions obtained for front velocities and the critical radius using Eq. **7**. Finally, length and time scales for deracemization are discussed.

Data, Materials, and Software Availability. Codes have been deposited on GitHub: https://github.com/GJeanULB/CSB-driven-by-diffusion.git (39).

ACKNOWLEDGMENTS. We thank the Fonds de la Recherche Scientifique–FNRS for financial support. J.G. is a Fonds pour la Formation à la Recherche dans l'Industrie et dans l'Agriculture (FRIA) grantee of the Fonds de la Recherche Scientifique–FNRS.

1. T. Buhse *et al.*, Spontaneous deracemizations. *Chem. Rev.* **121**, 2147–2229 (2021).
2. G. Laurent, D. Lacoste, P. Gaspard, Emergence of homochirality in large molecular systems. *Proc. Natl. Acad. Sci. U.S.A.* **118**, e2012741118 (2021).
3. M. Inaki, J. Liu, K. Matsuno, Cell chirality: Its origin and roles in left–right asymmetric development. *Philos. Trans. R. Soc. B Biol. Sci.* **371**, 20150403 (2016).
4. E. L. Eliel, S. H. Wilen, *Stereochemistry of Organic Compounds* (Wiley India Pvt Limited, 2008).
5. L. Riccardi *et al.*, Dynamic origin of chirality transfer between chiral surface and achiral ligand in Au38 clusters. *ACS Nano* **13**, 7127–7134 (2019).
6. C. Weiss, D. I. Sharapa, A. Hirsch, Coronenohelicenes with dynamic chirality. *Chem. Eur. J.* **26**, 14100–14108 (2020).
7. W. A. Bonner, The origin and amplification of biomolecular chirality. *Orig. Life Evol. Biosph.* **21**, 59–111 (1991).
8. A. Guijarro, M. Yus, *The Origin of Chirality in the Molecules of Life: A Revision from Awareness to the Current Theories and Perspectives of This Unsolved Problem* (Royal Society of Chemistry, 2008).
9. K. Soai, Asymmetric autocatalysis. Chiral symmetry breaking and the origins of homochirality of organic molecules. *Proc. Jpn. Acad. Ser. B Phys. Biol. Sci.* **95**, 89–110 (2019).

10. K. H. Ernst, Amplification of chirality at solid surfaces. *Orig. Life. Evol. Biosph.* **40**, 41 (2009).
11. K. Soai, S. Niwa, H. Hori, Asymmetric self-catalytic reaction. Self-production of chiral 1-(3-pyridyl)alkanols as chiral self-catalysts in the enantioselective addition of dialkylzinc reagents to pyridine-3-carbaldehyde. *J. Chem. Soc., Chem. Commun.* 982–983 (1990).
12. C. Viedma, Chiral symmetry breaking during crystallization: Complete chiral purity induced by nonlinear autocatalysis and recycling. *Phys. Rev. Lett.* **94**, 065504 (2005).
13. I. Baglai, M. Leeman, R. M. Kellogg, W. L. Noorduin, A Viedma ripening route to an enantiopure building block for Levetiracetam and Brivaracetam. *Org. Biomol. Chem.* **17**, 35–38 (2019).
14. Q. Cheng, Q. Ma, H. Pei, Z. Mo, Chiral membranes for enantiomer separation: A comprehensive review. *Sep. Purif. Technol.* **292**, 121034 (2022).
15. N. M. Maier, P. Franco, W. Lindner, Separation of enantiomers: Needs, challenges, perspectives. *J. Chromatogr. A* **906**, 3–33 (2001).
16. H. Lorenz, A. Seidel-Morgenstern, Processes to separate enantiomers. *Angew. Chem. Int. Ed.* **53**, 1218–1250 (2014).
17. T. J. Ward, K. D. Ward, Chiral separations: A review of current topics and trends. *Anal. Chem.* **84**, 626–635 (2012).
18. T. Aoki, Ki. Shinohara, T. Kaneko, E. Oikawa, Enantioselective permeation of various racemates through an optically active poly1-[dimethyl(10-pinanyl)silyl]-1-propyne membrane. *Macromolecules* **29**, 4192–4198 (1996).
19. Š. Hovorka *et al*., Permeability and diffusion coefficients of single methyl lactate enantiomers in Nafion® and cellophane membranes measured in diffusion cell. *Separa. Purif. Technol.* **158**, 322–332 (2016).
20. D. Frezzato, G. J. Moro, C. Zannoni, Molecular diffusion in liquid crystals and chiral discrimination. *I. Theory. J. Chem. Phys.* **122**, 164904 (2005).
21. D. Frezzato, C. Zannoni, G. J. Moro, Molecular diffusion in liquid crystals and chiral discrimination II. Model calculations.. *J. Chem. Phys.* **125**, 104903 (2006).
22. J. Jiang, D. K. Yang, Chirality differentiation by diffusion in chiral nematic liquid crystals. *Phys. Rev. Applied* **7**, 014014 (2017).
23. Y. Shin, Q. Wang, D. K. Yang, Chiral differentiation of limonene in chiral nematic liquid crystals. *Soft Matter* **16**, 3669–3677 (2020).
24. Y. Saito, H. Hyuga, Colloquium: Homochirality: Symmetry breaking in systems driven far from equilibrium. *Rev. Mod. Phys.* **85**, 603–621 (2013).
25. J. Gillet, L. Rongy, Y. De Decker, Spontaneous mirror symmetry breaking in reaction–diffusion systems: Ambivalent role of the achiral precursor. *Phys. Chem. Chem. Phys.* **24**, 26144–26155 (2022).
26. D. Hochberg, M. P. Zorzano, Reaction-noise induced homochirality. *Chem. Phys. Lett.* **431**, 185–189 (2006).
27. R. Plasson, A. Brandenburg, Homochirality and the need for energy. *Orig. Life. Evol. Biosph.* **40**, 93–110 (2010).
28. D. K. Kondepudi, G. W. Nelson, Chiral-symmetry-breaking states and their sensitivity in nonequilibrium chemical systems. *Phys. A: Stat. Mech. Appl.* **125**, 465–496 (1984).
29. F. C. Frank, On spontaneous asymmetric synthesis. *Biochim. Biophys. Acta* **11**, 459–463 (1953).
30. C. Blanco *et al*., Spontaneous emergence of chirality in the limited enantioselectivity model: Autocatalytic cycle driven by an external reagent. *ChemPhysChem* **14**, 2432–2440 (2013).
31. R. Plasson, H. Bersini, A. Commeyras, Recycling frank: Spontaneous emergence of homochirality in noncatalytic systems. *Proc. Natl. Acad. Sci. U.S.A.* **101**, 16733–16738 (2004).
32. Y. Saito, H. Hyuga, Chirality selection in open flow systems and in polymerization. *J. Phys. Soc. Jpn.* **74**, 1629–1635 (2005).
33. Y. Saito, H. Hyuga, Chirality selection in crystallization. *J. Phys. Soc. Jpn.* **74**, 535–537 (2005).
34. A. S. Mikhailov, *Foundations of Synergetics I, Springer Series in Synergetics*, H. Haken, Ed. (Springer, Berlin, Heidelberg, 1994), vol. 51.
35. A. Hagberg, E. Meron, Pattern formation in non-gradient reaction-diffusion systems: The effects of front bifurcations. *Nonlinearity* **7**, 805–835 (1994).
36. C. Dressel, T. Reppe, M. Prehm, M. Brautzsch, C. Tschierske, Chiral self-sorting and amplification in isotropic liquids of achiral molecules. *Nat. Chem.* **6**, 971–977 (2014).
37. C. Blanco, J. M. Ribó, D. Hochberg, Modeling spontaneous chiral symmetry breaking and deracemization phenomena: Discrete versus continuum approaches. *Phys. Rev. E* **91**, 022801 (2015).
38. M. Uwaha, H. Katsuno, Mechanism of chirality conversion of crystals by Viedma ripening and temperature cycling. *J. Cryst. Growth* **598**, 126873 (2022).
39. J. Gillet, GJeanULB/CSB-driven-by-diffusion. Github. https://github.com/GJeanULB/CSB-driven-by-diffusion. Deposited 16 February 2024.
40. V. Avetisov, V. Goldanskii, Mirror symmetry breaking at the molecular level. *Proc. Natl. Acad. Sci. U.S.A.* **93**, 11435–11442 (1996).